HHS Public Access

Author manuscript

Technology (Singap World Sci). Author manuscript; available in PMC 2016 December 01.

Published in final edited form as:

Technology (Singap World Sci). 2015 December ; 3(4): 179–188. doi:10.1142/S2339547815500065.

Scaffold-integrated microchips for end-to-end *in vitro* tumor cell attachment and xenograft formation

Jungwoo Lee[1,4], **Nathaniel Kohl**[2], **Sachin Shanbhang**[2], and **Biju Parekkadan**[1,3]

[1]Center for Engineering in Medicine, Massachusetts General Hospital & Harvard Medical School and Shriners Hospital for Children, Boston, MA 02114, USA

[2]Department of Scientific Computing, Florida State University, Tallahassee, FL 32306, USA

[3]Harvard Stem Cell Institute, Boston, MA 02138, USA

[4]Department of Chemical Engineering, University of Massachusetts, Amherst, MA 01003, USA

Abstract

Microfluidic technologies have substantially advanced cancer research by enabling the isolation of rare circulating tumor cells (CTCs) for diagnostic and prognostic purposes. The characterization of isolated CTCs has been limited due to the difficulty in recovering and growing isolated cells with high fidelity. Here, we present a strategy that uses a 3D scaffold, integrated into a microfludic device, as a transferable substrate that can be readily isolated after device operation for serial use *in vivo* as a transplanted tissue bed. Hydrogel scaffolds were incorporated into a PDMS fluidic chamber prior to bonding and were rehydrated in the chamber after fluid contact. The hydrogel matrix completely filled the fluid chamber, significantly increasing the surface area to volume ratio, and could be directly visualized under a microscope. Computational modeling defined different flow and pressure regimes that guided the conditions used to operate the chip. As a proof of concept using a model cell line, we confirmed human prostate tumor cell attachment in the microfluidic scaffold chip, retrieval of the scaffold en masse, and serial implantation of the scaffold to a mouse model with preserved xenograft development. With further improvement in capture efficiency, this approach can offer an end-to-end platform for the continuous study of isolated cancer cells from a biological fluid to a xenograft in mice.

INNOVATION

Microfluidic devices have been effective in capturing rare circulating tumor cells from blood and other biological fluids. Yet, the culture and expansion of captured tumor cells remains a challenge because of the inability to easily retrieve cells from a device. In this report, we introduce an innovative strategy to integrate a 3D hydrogel scaffold into a microfluidic device, whereby the scaffold can be retrieved after microfluidic cell attachment for serial *in vitro* or *in vivo* analysis. This scaffold-integrated chip can enable the characterization of isolated circulating tumor cells when optimally combined with cell-specific capturing techniques.

Correspondence should be addressed to B.P. (biju_parekkadan@hms.harvard.edu) and J.L. (jungwoo@engin.umass.edu).

INTRODUCTION

Microfluidic platforms have emerged as a powerful tool for studying cancer biology, particularly by capturing rare circulating tumor cells (CTCs) from patient blood samples[1–4]. Microfluidic captured CTCs have value for diagnostic and therapeutic applications in medicine since CTCs are considered precursor metastatic cells that contribute to 90% of cancer-associated death[5]. Various microfluidic platforms have been actively developed to enhance CTC-capture efficiency, purity and throughput. These platforms have already started to bring new understanding to human cancer and potentially patient care[6–10]. The functional characterization of microfluidically captured CTCs holds great promise to create patient-specific tumor cell lines and xenograft models to evaluate cancer heterogeneity and explore personalized medicine[11,12]. Yet, despite substantial technological advances, microfluidic captured tumor cells are difficult to retrieve from device without disrupting the cell's physiological state. The downstream characterization of CTCs *ex vivo* or in tumorigenic xenograft models *in vivo* is limited.

Recently a few studies have demonstrated the feasibility of CTC expansion by optimizing cell culture environments. For instance, Zhang *et al*. introduced fibroblasts and extracellular matrix (ECM) proteins into a microfluidic chip right after capturing CTCs that improved *ex vivo* proliferation of tumor cells[13]. Yu *et al*. also reported that serum free medium, human-derived growth factors, hypoxia, and non-adhesive substrates synergistically improved *ex vivo* culture of CTCs[14]. These results indicate that engineering cellular microenvironments would be an effective strategy to promote the survival and growth of CTCs. Biomaterials have been also introduced into microfluidic devices to help create an *in vivo*-like environment for captured CTCs[15–19]. These biomaterial-microfluidic platforms exhibit excellent fluidic control and have significantly improved the survival and function of captured CTCs. However, these integrated biomaterials cannot be separated from encased microfluidic devices making it restrictive for downstream functional analysis. In the field of tissue engineering, three-dimensional cell culture matrices (also known as scaffolds) have been widely used to mimic natural functions of ECM including structural support, mechanical and biochemical cues, and molecular gradients[20,21]. Its porous geometry accommodates a large number of cells, directs multicellular organization, and subsequently promotes the acquisition of differentiated tissue-level function[22,23]. Importantly, the freestanding nature of scaffolds allows easy integration into macro-bioreactors and/or *in vivo* models to create functional tissue analogues[24,25]. Scaffolds can be easily retrieved after bioreactor operation[26] and *in vivo* implantation for subsequent studies[27]. Yet, macro-bioreactor scaffolds are poor in fluidic control and *in situ* imaging when compared to microfluidic platforms, which limits their application for CTC capture platforms.

In this report, we introduce a new strategy to study CTCs by integrating a 3D hydrogel scaffold into a microfluidic device that can be retrieved after perfusion for downstream functional analysis. We focus on prostate tumors as a leading cause of death in adult men with a high propensity for bone metastasis[28] and used a prostate tumor cell line as a model system for cell attachment and xenograft formation. The strategy to integrate a 3D hydrogel scaffold into a microfluidic device is simple; we exploited an intrinsic property of hydrogel to expand into a microfluidic chamber after going from a dehydration/hydration cycle once

in contact with fluid. The microfluidic cell culture could be visualized under a microscope and, after use, the scaffold inside could be retrieved for serial implantation and *in vivo* analysis. In this study, we focused on understanding the operating conditions to isolate a tumor cell line in a microfluidic 3D hydrogel structure. Tumor cells, that were isolated in the scaffold, were retrieved and implanted into mice as a direct extension to create a functional xenograft. The presented approach is readily applicable to other hydrogel scaffolds with structural and material diversity to provide tissue-specific 3D microstructures with relevant ECM components for microfluidic cancer research.

RESULTS

Modular design of a scaffold-integrated microfluidic platform

Two modules, a porous hydrogel scaffold and a PDMS-based fluidic chamber, were independently manufactured before being merged together in a final micro-reactor design. Hydrogel scaffolds were synthesized in polyacrylamide using a template-fabrication method to provide a standardized matrix that is mechanical stabile, optically transparent, and highly porous to accommodate molecular and cellular transport[29,30]. The macroscopic dimension of a fully hydrated hydrogel scaffold was 6.7 ± 0.14 mm diameter and ∼1.5 mm thickness consisting of regularly arranged and interconnected uniform size spherical cavities (D = 208 ± 15 μm). The cavity surfaces were coated with type I collagen to improve cell adhesion (Fig. 1a). Hydrogel scaffolds reversibly undergo substantial volume change in response to hydration. For example, hydrogel scaffolds immersed in 100% ethanol shrink to 4.0 ± 0.92 mm in diameter and ∼0.6 mm in thickness, which corresponds to ∼78% volume reduction compared with its fully hydrated state. Rehydrated scaffolds can recover their hydrated state dimension, optical transparency, and mechanical durability even after more than 10 rounds of dehydration and rehydration (Fig. 1b). We exploited these intrinsic properties to integrate a hydrogel scaffold into a PDMS-based bioreactor. The reduced size of a dehydrated hydrogel scaffold made it easy to be inserted in a cylindrically shaped PDMS chamber that has slightly smaller dimension than a fully hydrated hydrogel scaffold (D = 6 mm, H = 1 mm). This bioreactor with an inserted scaffold could then sealed onto a glass slide and bonded with oxygen plasma. Priming of the device with deionized water rapidly rehydrated the enclosed hydrogel scaffold, which expanded to completely fill the PDMS chamber space leaving no dead volume (Fig. 1c, **Supplementary Video 1**[a]).

Transport characteristics of scaffold-integrated microfluidic bioreactor

The scaffold provides a tortuous, high surface-area-to-volume platform similar to a tissue ECM. Before introducing cells, we systematically characterized hydrodynamic microenvironments created within the integrated hydrogel scaffold. Taking advantage of the regular porous structure, we used the lattice Boltzmann method to simulate the complex microflow corresponding to three different bulk flow rates (Q = 10, 50 and 100 μL/min). In the simulation, inter-connected cavities in the hydrogel were arranged on a regular face-centered cubic lattice[31], and the velocity field inside the scaffold was determined at different

[a]Supplementary Video 1 (“Rehydration of a PDMS chip inserted dehydrated scaffold via infusing PBS”) can be viewed at http://www.worldscientific.com/doi/suppl/doi:10.1142/S2339547815500065

bulk flow rates. As shown in Fig. 2a, the computational modeling revealed that the fluid rushes into a cavity from an inter-connecting channel, glides across the core of the cavity, and rushes out via a channel to an adjacent cavity. As the bulk flow rate was increased, the spatial heterogeneity of the velocity field also increased, and the contrast between the fast microflow near the channels and the slow microflow near the cavity surface became sharper. In addition, the simulation results revealed that the flow rate positively correlates with the perfused space, and negatively with the perfusion uniformity. The model also indicated the formation of local stagnation points that preferentially formed near the cavity surface adjacent to inter-connecting channels. We computed the mechanical shear stress profiles in the fluid perfused regions of the scaffold (Fig. 2b) and found that the regions of high stress are correlated with regions of strong velocity gradients, near the entrance of inter-connecting channels. For Q = 10 μL/min, the magnitude of the shear stress at the center of cavities is of the order of 0.1 megapascal (MPa). The stress at the cavity walls is about 10 times larger, ∼1 MPa. The stresses are largest in the interconnecting pores, as the fluid is forced through narrow constrictions. Here the magnitude of the shear stress is about 100 times larger (∼10 MPa) than the bulk. The magnitude of the stress is approximately proportional to the flow rate; thus, for example, the shear stress at the cavity center at Q = 100 μL/min is approximately 1 MPa. Collectively these data suggest that cells adherent on the cavity surface would not undergo high shear and could remain adherent while being exposed to convective delivery of macromolecules within the solution.

These simulations were experimentally tested in microreactors and monitored under an optical microscope that allowed direct observation of dynamic transport phenomena through a transparent hydrogel matrix. An enclosed hydrogel scaffold retained its interconnected macroscopic channels for bulk flow, with moderate deformation of the cavity size due to the pressure. Overall pore size was reduced as 154 ± 45 μm and we observed different pore diameter distribution in the central (125 ± 41 μm) and marginal (173 ± 45 μm) regions (Supplementary Fig. 1); while the simulations modeled the hydrogel as a non-deformable material, this experimental observation is consistent with the pressure and stress profiles observed in the model. In addition, the hydrogel scaffold provides subcellular scale pores (2.37 ± 0.45 μm) in the hydrogel matrix that could be used for small molecule transport (Fig. 3a). We first analyzed the perfusion profile of cellular size (D ∼10 μm) fluorescent polymeric microparticles under controlled pressure-driven flow. Most microparticles passed through open porous microstructures in the hydrogel scaffold as forming meandering streamlines, while some particles deviated from the streamlines and became trapped in stagnation points that were found at the varying diameters of convoluted channels as predicted by the model (**Supplementary Video 2**[b]). The trajectory of individual particle movement was captured by increasing exposure time of a fluorescent microscope (Fig. 3b), which allowed quantitative and qualitative comparison of inter-scaffold perfusion profiles as a function of flow rate (Fig. 3c).

We then examined the perfusion profile of small molecules using a rhodamine solution under gravity-induced flow (i.e. 39 μL/min in an empty chamber) and compared transport

[b]Supplementary Video 2 (“Perfusion profile of cellular size microparticles perfusion at 10 μL/min) can be viewed at http://www.worldscientific.com/doi/suppl/doi:10.1142/S2339547815500065

phenomenon with an empty chamber or a chamber with a bulk hydrogel disc inserted that had only subcellular scale pores. As shown in Fig. 3d, the fluid entering into an empty chamber remained centralized initially with little edge dispersion, but soon converged at the outlet. The fluid entering into a scaffold-reactor continuously branched to the edges by passing while creeping through the micro-porous structure. Pressure gradients from the edge to the center, as suggested by the modeling, could account for the edge dispersion of the fluid stream along the lines of least resistance. In both cases, the entire chamber was eventually perfused by rhodamine solution in 5 minutes. However, during the same period no significant flow was made in a bulk hydrogel chamber due to the high hydraulic resistance. After washing, we observed significantly extended retention time of dye molecules in a scaffold chamber compared to an empty chamber. The relative flow rate of hydrogel scaffold chambers reached about 90% of empty chambers (Fig. 3e). These results indicate that the differential porous structure in hydrogel scaffolds created two different hydrodynamic regimes with 90% bulk flow via microscale pores and the remaining 10% flow via subcellular scale pores in the hydrogel matrix. These data provided confidence in operating the device under the specific range of flow rates (0.5–100 μL/min) during seeding and culture, while also validating the use of computational modeling to predict further insight into any future modifications of the bioreactor.

Attachment of tumor cells in scaffold chips with and without a feeder layer

As a proof-of-concept, PC3 human prostate tumor cells were evaluated for engraftment in the scaffold using a protocol guided by our modeling flow simulations (Fig. 4a). PC3 cells were engineered with a luciferase and green fluorescent protein reporter (Luc-GFP PC3) to microscopically distinguish tumor cells in the scaffold and also quantitatively determine the growth of tumor cells. Infused Luc-GFP PC3 cells (5×10^4 cells in 1 mL at 20 μL/min) traveled following sinusoid-like pore channels and randomly attached to the scaffold within the device. Using this method, cancer cell capture efficiency was ∼55% and microfluidically captured cells remained viable for at least 3 days under continued chip perfusion at (Fig. 4b). These data indicated that the porous hydrogel matrix coated with ECM was sufficient to capture cancer cells.

A separate study was designed to explore if pre-coating the scaffold with a feeder layer of human bone marrow stromal cells (BMSCs), which are known to support PC3 cell function, would impact engraftment. Based on the result of particle perfusion studies, we developed a cell seeding protocol using single, rapid infusion of a concentrated cell suspension (5×10^5 BMSCs in 200 μL) for more uniform dispersion and coverage (Fig. 4c). The mechanically durable hydrogel retained its physical integrity during high flow rate conditions, which is challenging in other soft hydrogel-based fluidic channels e.g. collagen and alginate. The density of cell suspension was determined according to the estimated surface area provided by the enclosed hydrogel scaffold that is about 35 times larger than an empty chamber where only the bottom surface is available for cell adhesion (Supplementary Fig. 2). We achieved around 80% cell seeding efficiency using this method (Supplementary Fig. 3). Live/dead staining after 24 hours of perfusion culture showed over 90% cell viability (Supplementary Fig. 4). Confocal Z-stack images confirmed that BMSCs distributed and adhered in both axial and transverse directions within a scaffold-chip (Fig. 4d). Tumor cells were then

infused to create a co-culture. Adhesion and proliferation of captured Luc-GFP PC3 cells interacting with BMSCs during perfusion culture was easily monitored (Fig. 4e) and some of them stuck to the BMSCs (Fig. 4f, **Supplementary Video 3**[C]). There was no significant improvement in engraftment efficiency with the use of a feeder layer.

Retrieval of bioreactor-primed scaffolds for direct *in vivo* implantation

A distinguishing feature of the modular scaffold-integrated microreactor design is that a prepared 3D microenvironment can be retrieved intact for continuous *in vitro* and *in vivo* functional analysis after reactor operation (Fig. 5a). Retrieved microfluidically engrafted tumor cells with or without a stromal coating could be maintained in a standard well plate that allowed quantitative monitoring stromal dependent tumor-specific growth using bioluminescence (Fig. 5b). In this format, it was observed that BMSC scaffolds significantly enhanced PC3 tumor cell growth. The culture can be continued until the available surface area is fully covered by tumor and stromal cells. Scanning electron microscope images of 3 weeks *in vitro* cultured scaffolds showed a fully covered pore surface that exhibited quite distinct morphology between tumor-only culture and tumor-stromal co-culture (Fig. 5c). This stromal-enhanced growth was not seen in control co-cultures on 2D tissue culture plastic, which suggests the importance of a 3D environment for stromal-support of PC3 prostate tumor cell growth (Supplementary Fig. 5). We could also retrieve and directly implant microfluidically prepared tumor-stroma co-cultures *in vivo* that enabled both qualitative and quantitative analysis of stromal-dependent tumor development using whole-body bioluminescent imaging (Fig. 5d). The scaffolds, inoculated with PC3 cells, formed xenografts after subdermal implantation in immunodeficient NSG mice. Although BMSC-scaffolds showed moderately enhanced engraftment profiles compared to stromal-free scaffolds, no significant difference was observed due to the large deviation (Fig. 5e). Gross images of explanted scaffolds after 7 weeks implantation provide the feasibility of an integrated device that can microfluidically prepare cells in scaffold for direct *in vivo* implantation (Fig. 5f).

DISCUSSION

In this study, we presented an integrative approach to link *in vitro* tumor cell capture and *in vivo* implantation using a modular designed microfluidic hydrogel scaffold. Although biomaterials have been applied with microfluidic platforms to provide *in vivo*-like 3D extracellular milieu[18,32–35], the cells cannot easily be separated from the biomaterial for continuous functional analysis *ex vivo* and/or *in vivo*. The key innovation here was the integration of a mechanically durable synthetic hydrogel scaffold within a PDMS fluidic device as a transferable matrix. A porous polyacrylamide hydrogel maintained structural integrity after dehydration, rehydration, and high pulsatile flow during cell seeding. These features are critical for microfluidic integration and uniform cell dispersion. A nonuniformity in pressure differences that was observed in our studies could be improved with a more rigid structure or even leveraged for inducing differential mechanical signaling

[C]Supplementary Video 3 (“Infusing PC3 cancer cell suspension at 10 μL/min to a BMSC growing microfluidic hydrogel scaffold“) can be viewed at http://www.worldscientific.com/doi/suppl/doi:10.1142/S2339547815500065

in the same scaffold without compartmentalization. The standardized 3D microstructure that was formed by the template-based synthesis was amenable to computational modeling and predictable flow conditions. In addition, the hierarchical porous structure exhibited physiologically relevant mass transport as accommodating both bulk flow (90%) by the macroscopic channels that connect each cavity within the scaffold and diffusion flow (10%) in subcellular pores in hydrogel matrix itself. This specific 3D porous hydrogel scaffold has been used for *in vitro* and *in vivo* bone marrow tissue engineering and cancer research applications[29,36–39]. Here, we have created a microfluidic chamber for scaffold culture and applied it as a microfluidic tumor cell attachment and implantation substrate. The presented approach could be also evolved with different biomaterials to expand the structural and material diversity of microenvironments in response to a user's desired application.

There are a number of areas where the technology can be improved, particularly in the sensitive and specific capture of such rare cells. Many microfluidic capture technologies have primarily focused on improving capture efficiency in the context of inherently low number of CTCs[40,41]. Our model system studies did not consider these important considerations of primary tumor cells, the presence of blood, low isolated cell numbers, and capture efficiency. Instead, we focused on the downstream growth of CTCs in a single microfluidic platform that can stabilize subsequent culture to amplify CTC number *ex vivo* and facilitate recovery and characterization. This first-generation chip had robust colonization and implantation results using a model prostate cell line and provided confidence in moving forward with blood experimental samples under ethical and regulatory guidelines of human subjects research. The selective capture of cells from biological samples in the scaffold on-chip could facilitate targeted growth *ex vivo* and subsequent *in vivo* testing. In the current design of microfluidic hydrogel scaffolds, CTC-capture was largely determined by contoured channel geometry that generated stagnation points. Our results suggest that the adherence of prostate tumor cells was a function of the collagen coating and microstructure of the scaffolds and was not improved by a prestromalized scaffold. Yet, a stromal coating did significantly promote the proliferation of adhered tumor cells both *in vitro* and *in vivo* suggesting that a tailored microenvironment can encourage growth after cell capture. The use of selective antibodies, pre-coated tissue beds, and enlarged chip dimensions may collectively enhance the ability to capture and concentrate CTCs. Currently, scaffolds are irreversibly integrated into a PDMS chamber by an oxygen-plasma treatment. Thus, the retrieval process required manual cutting of PDMS that could damage the co-culture environment in the hydrogel scaffolds. Reversible bonding or encasing methods[42,43] could be developed to improve and potentially automate the intact recovery of tumor-cell captured scaffolds.

Diagnostic and drug testing assays are also envisioned using this integrated platform. The technology we have described is designed to complement CTC capture approaches with a non-destructive method to retrieve cells isolated in a device for post-hoc expansion, analysis, or transfer into an animal model for *in vivo* functional testing. Patient-specific xenografts could be created with this direct implantation method to serve as a companion model for monitoring tumor progression and drug efficacy during clinical trials. These microfluidic hydrogel scaffolds can also have value in understanding basic cancer biology

and progression in a 3D environment upon capture[33,34,44–47]. Besides cancer research, the microfluidic hydrogel scaffolds can be applied for capturing other clinically important rare cells or infectious pathogens to monitor their dynamic progression.

The preparation of microscale tissues for unimpeded *in vivo* use could also benefit from this technology. The encased hydrogel scaffold significantly increased the available surface area for cell adhesion by 35-times when compared to an empty chamber in which only bottom surface is available for cell adhesion. This increased surface area, combined with a highly porous structure for mass transport, can enable a relatively dense cell culture. We and other investigators have made arrays of spherical microcavities in PDMS for the spheroid culture of cancer cells that permit explicit characterization of fluid transport and co-culture under defined conditions [48–51]. The *in vivo* integration of these arrayed spheroid cultures is difficult. Using parallel processing, multiple tissues on-chip could be merged together for a larger and uniform graft with optimal nutrient delivery achieved at the smaller unit scale. Engineered microtissue units can be assembled after retrieval to make a patient-specific size and shape of a multicellular 3D organization with tissue-level functionality. Additional structural and cellular complexity, such as an embedded endothelium, may aid in accelerating functional engraftment *in vivo*. There is also an opportunity to dope biodegradable polymers into the scaffold materials that can degrade *in vivo* and provide space for the infiltration and remodeling of host cells with the implanted biomaterial over time.

In conclusion, we present a new approach to help characterize isolated tumor cells from a biological fluid by integrating a hydrogel scaffold matrix into a fluidic device. This hybrid technology can offer great flexibility in structural design and material selection to provide a diverse range of tissue-mimicking microenvironments in a microfluidic platform. A microfluidically isolated tumor scaffold was successfully built and directly implanted into mice with preserved xenograft capacity as a proof-of-concept. Taken together, we anticipate that this technology could contribute to the translation of CTC capture technologies and microphysiological tumor models for diagnostic and therapeutic applications.

MATERIALS AND METHODS

All chemicals and supplies were purchased from Sigma Aldrich or Fisher Scientific unless otherwise stated. All mouse and primary human cell experiments were reviewed and approved by an internal review board of Massachusetts General Hospital.

Microfluidic hydrogel scaffold fabrication

Polyacrylamide based inverted colloidal crystal hydrogel scaffolds (Pore $D = 250 \pm 30$ μm) were prepared following the previously reported method [29]. Macroscopic dimension of fully hydrated hydrogel scaffolds was about 6.5 mm diameter and 1.5 mm thickness. Type I collagen fibers were covalently immobilized on the pore surface utilizing an amine and photo-reactive heterobifunctional cross-linker (Sulfo-SANPH). PDMS based cylindrical chambers ($D = 6$ mm, $H = 1$ mm) were prepared by modifying a plastic master molding technique[52]. The overall dimension of a microchip was 20 mm × 15 mm × 5 mm (Length × Width × Height). Before PDMS integration, hydrogel scaffolds were dehydrated by

immersed in a 70% ethanol solution that substantially shrank the hydrogel scaffold volume while maintaining gel-like elasticity. After oxygen-plasma surface treatment of a PDMS chamber and a glass slide, a dehydrated scaffold was immediately inserted into the PDMS chamber, sealed with the glass slide and then placed on a hot plate at 60 °C for 10 minutes. Subsequently the PDMS chamber was perfused with deionized water that rehydrated the dehydrated hydrogel scaffold and also washed away remaining ethanol. The microfluidic hydrogel scaffold was further perfused with phosphate buffered saline (PBS) and stored at 4 °C until used.

Characterization of transport and hydrodynamic microenvironments

Acellular microfluidic hydrogel scaffolds were used to characterize hydrodynamic and transport microenvironment. Empty and a bulk hydrogel disc (6.5 mm diameter, ~1.5 mm thickness) inserted chambers were prepared following the procedure described above and used as controls. Rhodamine B solution (MW = 479) was passively infused into the microfluidic chips by gravitational force to simulate and also directly visualize small molecule transport phenomenon. The relative flow rate was determined by measuring the volume of eluted dye solution for 5 minutes. Polycapolacton based microparticles ($D \sim 10$ μm) including fluorescein isothiocyanate (FITC) were prepared by slightly modifying the previously reported single-emulsion droplet based microfluidics[53]. Fluorescent microparticles having similar dimension to floating cells were infused into the microfluidic hydrogel scaffold at three different flow rates i.e. 10, 50 and 100 μL/min using a syringe pump (New Era). Flow rate dependent perfusion profiles and the trajectory of individual particle movement were monitored under an inverted fluorescent microscope (Zeiss AxioVert 200).

Inter-pore perfusion profiles were simulated using a computational fluid dynamics method called the lattice Boltzmann method[54,55]. In this method, fictive particles undergo consecutive collision and propagation on a discrete mesh[56]. It is ideally suited to model complex internal boundaries represented by the hydrogel microstructure, due to local dynamics and particle nature of the method. Computations were implemented using the open-source PalaBos software on a D3Q19 mesh[57]. The model geometry consisted of cavities of 100 μm radius arranged on a face-centered cubic (FCC) lattice, connected by channels of 10 μm radius; 3 FCC unit cells in the *x*-direction and 2 FCC unit cells in the *y*- and *z*-directions were used. Periodic boundary conditions were employed in the *y*- and *z*-directions, while a pressure gradient was applied along the *x*-direction. No-slip boundary conditions were enforced at the cavity surfaces[58]. At the flow rates studied, the pressure gradient was proportional to the bulk flow rate, and we chose pressure gradients that yielded bulk flow rates of 10, 50 and 100 μL/min. The results of the computation were visualized using ParaView and VisIt visualization tool kits[59,60].

Microfluidic culture human prostate tumor cells and bone marrow stromal cells (BMSCs)

PC3 human prostate tumor cells were culture with medium composed of 10% fetal bovine serum and 1% penicillin and streptomycin (Gibco/Life Technologies) in Dulbecco's Modified Eagle's Medium. Stable Luciferin and green fluorescent genes-transduced PC3 cell line (Luc-GFP PC3) was generated using high titer bidirectional lentivirus as previously

described[61]; 5×10^4 Luc-GFP PC3 cells dispersed in 1 mL medium were infused into microfluidic chip at 20 μL/min. After incubation for 3 hours in a static condition, microfluidic chip was perfused with media at 0.2 μL/min using a 12-channel programmable syringe pump. Primary BMSCs were isolated from health donor's fresh bone marrow aspirate (Lonza) and expanded following the previously reported protocol[62]. BMSCs were cultured with medium composed of 15% fetal bovine serum, 100 U/mL penicillin, 100 μg/mL streptomycin, 20 mg/L gentamicin, 1 ng/L fibroblast growth factor, and 3 g/L sodium bicarbonate in alpha-minimum essential medium (α-MEM) at 37 °C with 10% CO_2 and 100% humidity. A dense BMSC suspension (1×10^6 cells in 200 μL) was rapidly infused into the microfluidic hydrogel scaffold by a single injection and then incubated for 3 hours in a static condition before starting medium perfusion at 0.2 μL per min using a 12-channel programmable syringe pump (New Era). After 3 days perfusion culture of human BMSCs, 5×10^4 Luc-GFP PC3 cells dispersed in 1 mL medium were infused into BMSC and acellular microfluidic hydrogel scaffolds at 20 μL/min. Subsequently tumor cells introduced microfluidic scaffolds were perfused at 0.2 μL/min. PC3 cancer cells and human BMSCs seeding efficiency was determined by counting cell number before and after infusion into a microfluidic hydrogel scaffold ($n = 5$).

Microscopic imaging

By serially infusing FITC-Dextran and deionized water, deformed pore structure of a hydrogel scaffold integrated into a PDMS chamber was visualized under a fluorescent microscope (Zeiss). After 24 hours human BMSCs seeding, calcein and ethidium homodimer-1 based live-dead staining dye solution (Invitrogen) was infused into the microfluidic hydrogel scaffold chip and cell viability was determined under a fluorescent microscope. Live-dead stained fluorescent images were further processed to quantitatively determine cell viability. For fluorescent imaging of human BMSC-PC3 co-culture, BMSCs were pre-stained with a 5-(and-6)-(((4-Chloromethyl)Benzoyl)Amino) Tetramethylrhodamine (CMTMR) cell tracker dye (541 nm Excitation/565 nm Emission) before introducing the microfluidic hydrogel scaffold. Luc-GFP PC3 cells were directly imaged using a GFP channel. For scanning electron microscope (SEM) imaging, microfluidic cultured scaffolds were retrieved from a PDMS chamber using a razor blade and immediately fixed in 2% glutaladehyde solution. Subsequently hydrogel scaffolds were serially dehydrated with 20, 50, 70, 90 and 100% ethanol solution, and further dried using a lyophilizer overnight. A thin platinum/gold film was deposited on the samples using a sputter coating machine (208HR, Cressington) and then imaged under Field Emission SEM Ultra55 (Zeiss).

In vitro and *in vivo* monitoring retrieved microfluidically-primed microenvironment

After 1-week perfusion culture of Luc-GFP PC3 tumor cells in an acellular and a BMSC-residing microfluidic chip, an integrated hydrogel scaffold was retrieved by cutting and then delaminating a PDMS from a glass slide. Although an integrated scaffold can be retrieved intact, this manual process could damage the scaffold that potentially damages co-culture environment. Retrieved hydrogel scaffolds were immediately placed in a 24-well plate and 500 μL of 1:10 diluted luciferin substrate (Promega) was loaded in each well. Bioluminescent signal from Luc-GFP PC3 cells was measured by a microplate reader

(BioTeck Synergy2) for 7 days with 2–3 days interval. As a control experiment, 500 Luc-GFP PC3 cells were cultured on a 24-well plate with and without BMSCs. The growth of tumor cells were determined by measuring bioluminescent signal for 11 days after loading 500 μL of 1:10 diluted luciferin substrate. In a separate experiment, retrieved scaffolds were subdermally implanted on the dorsal side of 8 week old NOD/SCID/IL2γ^{null} (NSG) male mice (Jackson Laboratory) following the previously reported method[29]. Typically 4 scaffolds were implanted in each mouse i.e. 2 from acellular and the other 2 from BMSC microfluidic hydrogel scaffolds. Post 1 and 5 weeks mice were imaged after intraperitoneal injection of 150 μL D-Luciferin bioluminescent substrate (Caliper Life Sciences) using an *In Vivo* Imaging System (IVIS-100) (Perkin Elmer) with constant settings throughout the entire experiment.

Statistics

Statistical comparisons of data were performed using SPSS version 17 software. Nonparametric tests, i.e. Kruskal-Wallis and Mann-Whitney tests, were applied for semi-quantitative image and bioluminescent signal analysis.

Supplementary Material

Refer to Web version on PubMed Central for supplementary material.

ACKNOWLEDGEMENTS

We give thanks to Prof. Daniel Irimia and Dr. Salil Desai for discussion about PDMS chamber design and plastic master mold fabrication, respectively. This work was supported by NIH Grants R01EB012521 (B.P.), K01DK087770 (B.P.), K99CA163671 (J.L.) and the Shriners Hospitals for Children (B.P., J.L.).

REFERENCES

1. Nagrath S, Sequist LV, Maheswaran S, Bell DW, Irimia D, et al. Isolation of rare circulating tumour cells in cancer patients by microchip technology. Nature. 2007; 450:1235–1239. [PubMed: 18097410]
2. Maheswaran S, Sequist LV, Nagrath S, Ulkus L, Brannigan B, et al. Detection of mutations in EGFR in circulating lung-cancer cells. New Engl. J. Med. 2008; 359:366–377. [PubMed: 18596266]
3. Esmaeilsabzali H, Beischlag TV, Cox ME, Parameswaran AM, Park EJ, et al. Detection and isolation of circulating tumor cells: Principles and methods. Biotechnol. Adv. 2013; 31:1063–1084. [PubMed: 23999357]
4. Ozkumur E, Shah AM, Ciciliano JC, Emmink BL, Miyamoto DT, et al. Inertial focusing for tumor antigen-dependent and -independent sorting of rare circulating tumor cells. Sci. Trans. Med. 2013; 5:179ra147.
5. Vanharanta S, Massague J. Origins of metastatic traits. Cancer Cell. 2013; 24:410–421. [PubMed: 24135279]
6. Li P, Stratton ZS, Dao M, Ritz J, Huang TJ. Probing circulating tumor cells in microfluidics. Lab Chip. 2013; 13:602–609. [PubMed: 23306378]
7. Chen J, Li J, Sun Y. Microfluidic approaches for cancer cell detection, characterization, and separation. Lab Chip. 2012; 12:1753–1767. [PubMed: 22437479]
8. Khoo BL, Warkiani ME, Tan DS, Bhagat AA, Irwin D, et al. Clinical validation of an ultra high-throughput spiral microfluidics for the detection and enrichment of viable circulating tumor cells. PloS One. 2014; 9:e99409. [PubMed: 24999991]

9. Gakhar G, Navarro VN, Jurish M, Lee GY, Tagawa ST, et al. Circulating tumor cells from prostate cancer patients interact with E-selectin under physiologic blood flow. PloS One. 2013; 8:e85143. [PubMed: 24386459]
10. Kang JH, Krause S, Tobin H, Mammoto A, Kanapathipillai M, et al. A combined micromagnetic-microfluidic device for rapid capture and culture of rare circulating tumor cells. Lab Chip. 2012; 12:2175–2181. [PubMed: 22453808]
11. Giuliano M, Herrera S, Christiny P, Shaw C, Creighton CJ, et al. Circulating and disseminated tumor cells from breast cancer patient-derived xenograft-bearing mice as a novel model to study metastasis. Breast Cancer Res. 2015; 17:3. [PubMed: 25572662]
12. Zhang X, Claerhout S, Prat A, Dobrolecki LE, Petrovic I, et al. A renewable tissue resource of phenotypically stable, biologically and ethnically diverse, patient-derived human breast cancer xenograft models. Cancer Res. 2013; 73:4885–4897. [PubMed: 23737486]
13. Zhang Z, Shiratsuchi H, Lin J, Chen G, Reddy RM, et al. Expansion of CTCs from early stage lung cancer patients using a microfluidic co-culture model. Oncotarget. 2014; 5:12383–12397. [PubMed: 25474037]
14. Yu M, Bardia A, Aceto N, Bersani F, Madden MW, et al. Cancer therapy. *Ex vivo* culture of circulating breast tumor cells for individualized testing of drug susceptibility. Science. 2014; 345:216–220. [PubMed: 25013076]
15. Bichsel CA, Gobaa S, Kobel S, Secondini C, Thalmann GN, et al. Diagnostic microchip to assay 3D colony-growth potential of captured circulating tumor cells. Lab Chip. 2012; 12:2313–2316. [PubMed: 22565166]
16. Jeon JS, Bersini S, Gilardi M, Dubini G, Charest JL, et al. Human 3D vascularized organotypic microfluidic assays to study breast cancer cell extravasation. Proc. Natl. Acad. Sci. USA. 2015; 112:214–219. [PubMed: 25524628]
17. Sung KE, Yang N, Pehlke C, Keely PJ, Eliceiri KW, et al. Transition to invasion in breast cancer: A microfluidic *in vitro* model enables examination of spatial and temporal effects. Integr. Biol. 2011; 3:439–450.
18. Rizvi I, Gurkan UA, Tasoglu S, Alagic N, Celli JP, et al. Flow induces epithelial-mesenchymal transition, cellular heterogeneity and biomarker modulation in 3D ovarian cancer nodules. Proc. Natl. Acad. Sci. USA. 2013; 110:E1974–E1983. [PubMed: 23645635]
19. Bischel LL, Beebe DJ, Sung KE. Microfluidic model of ductal carcinoma *in situ* with 3D, organotypic structure. BMC Cancer. 2015; 15:12. [PubMed: 25605670]
20. Lee J, Cuddihy MJ, Kotov NA. Three-dimensional cell culture matrices: State of the art. Tissue Eng. Part B Rev. 2008; 14:61–86. [PubMed: 18454635]
21. Khademhosseini A, Langer R, Borenstein J, Vacanti JP. Microscale technologies for tissue engineering and biology. Proc Natl. Acad. Sci. USA. 2006; 103:2480–2487. [PubMed: 16477028]
22. Griffith LG, Swartz MA. Capturing complex 3D tissue physiology *in vitro* . Nat. Rev. Mol. Cell. Biol. 2006; 7:211–224. [PubMed: 16496023]
23. Nelson CM, Bissell MJ. Of extracellular matrix, scaffolds, and signaling: Tissue architecture regulates development, homeostasis, and cancer. Annu. Rev. Cell Dev. Biol. 2006; 22:287–309. [PubMed: 16824016]
24. Ma PX. Biomimetic materials for tissue engineering. Adv. Drug Deliv. Rev. 2008; 60:184–198. [PubMed: 18045729]
25. Chen AA, Thomas DK, Ong LL, Schwartz RE, Golub TR, et al. Humanized mice with ectopic artificial liver tissues. Proc. Natl. Acad. Sci. USA. 2011; 108:11842–11847. [PubMed: 21746904]
26. Lee J, Kotov NA. Notch ligand presenting acellular 3D microenvironments for *ex vivo* human hematopoietic stem-cell culture made by layer-by-layer assembly. Small. 2009; 5:1008–1013. [PubMed: 19334013]
27. Torisawa YS, Spina CS, Mammoto T, Mammoto A, Weaver JC, et al. Bone marrow-on-a-chip replicates hematopoietic niche physiology *in vitro* . Nat. Methods. 2014; 11:663–669. [PubMed: 24793454]
28. Sturge J, Caley MP, Waxman J. Bone metastasis in prostate cancer: Emerging therapeutic strategies. Nat. Rev. Clin. Oncol. 2011; 8:357–368. [PubMed: 21556025]

29. Lee J, Li M, Milwid J, Dunham J, Vinegoni C, et al. Implantable microenvironments to attract hematopoietic stem/cancer cells. Proc. Natl. Acad. Sci. USA. 2012; 109:19638–19643. [PubMed: 23150542]
30. Lee J, Shanbhag S, Kotov N. Inverted colloidal crystals as three-dimensional microenvironments for cellular co-cultures. J. Mater. Chem. 2006; 16:3558–3564.
31. Shanbhag S, Wang S, Kotov NA. Cell distribution profiles in three-dimensional scaffolds with inverted-colloidal-crystal geometry: Modeling and experimental investigations. Small. 2005; 1:1208–1214. [PubMed: 17193421]
32. Jeon JS, Bersini S, Whisler JA, Chen MB, Dubini G, et al. Generation of 3D functional microvascular networks with human mesenchymal stem cells in microfluidic systems. Integr. Biol. 2014; 6:555–563.
33. Seo BR, Delnero P, Fischbach C. *In vitro* models of tumor vessels and matrix: engineering approaches to investigate transport limitations and drug delivery in cancer. Adv. Drug Deliv. Rev. 2014; 69–70:205–216.
34. Bersini S, Jeon JS, Dubini G, Arrigoni C, Chung S, et al. A microfluidic 3D *in vitro* model for specificity of breast cancer metastasis to bone. Biomaterials. 2014; 35:2454–2461. [PubMed: 24388382]
35. Hsu YH, Moya ML, Hughes CC, George SC, Lee AP. A microfluidic platform for generating large-scale nearly identical human microphysiological vascularized tissue arrays. Lab Chip. 2013; 13:2990–2998. [PubMed: 23723013]
36. Nichols JE, Cortiella J, Lee J, Niles JA, Cuddihy M, et al. *In vitro* analog of human bone marrow from 3D scaffolds with biomimetic inverted colloidal crystal geometry. Biomaterials. 2009; 30:1071–1079. [PubMed: 19042018]
37. Bersani F, Lee J, Yu M, Morris R, Desai R, et al. Bioengineered implantable scaffolds as a tool to study stromal-derived factors in metastatic cancer models. Cancer Res. 2014; 74:7229–7238. [PubMed: 25339351]
38. Long TJ, Sprenger CC, Plymate SR, Ratner BD. Prostate cancer xenografts engineered from 3D precision-porous poly(2-hydroxyethyl methacrylate) hydrogels as models for tumorigenesis and dormancy escape. Biomaterials. 2014; 35:8164–8174. [PubMed: 24942815]
39. Cuddihy MJ, Wang Y, Machi C, Bahng JH, Kotov NA. Replication of bone marrow differentiation niche: Comparative evaluation of different three-dimensional matrices. Small. 2013; 9:1008–1015. [PubMed: 23281196]
40. Karabacak NM, Spuhler PS, Fachin F, Lim EJ, Pai V, et al. Microfluidic, marker-free isolation of circulating tumor cells from blood samples. Nat. Protoc. 2014; 9:694–710. [PubMed: 24577360]
41. Deng Y, Zhang Y, Sun S, Wang Z, Wang M, et al. An integrated microfluidic chip system for single-cell secretion profiling of rare circulating tumor cells. Sci. Rep. 2014; 4:7499. [PubMed: 25511131]
42. Harris J, Lee H, Vahidi B, Tu C, Cribbs D, et al. Non-plasma bonding of PDMS for inexpensive fabrication of microfluidic devices. J. Vis. Exp. 2007; 9:410. [PubMed: 18989450]
43. Ward A, Quinn KP, Bellas E, Georgakoudi I, Kaplan DL. Noninvasive metabolic imaging of engineered 3D human adipose tissue in a perfusion bioreactor. PloS One. 2013; 8:e55696. [PubMed: 23405199]
44. Park JY, Takayama S, Lee SH. Regulating microenvironmental stimuli for stem cells and cancer cells using microsystems. Integr. Biol. 2010; 2:229–240.
45. Song JW, Cavnar SP, Walker AC, Luker KE, Gupta M, et al. Microfluidic endothelium for studying the intravascular adhesion of metastatic breast cancer cells. PloS One. 2009; 4:e5756. [PubMed: 19484126]
46. Sung KE, Beebe DJ. Microfluidic 3D models of cancer. Adv. Drug Deliv. Rev. 2014; 79–80:68–78.
47. Moya M, Tran D, George SC. An integrated *in vitro* model of perfused tumor and cardiac tissue. Stem Cell Res. Ther. 2013; 4(Suppl 1):S15. [PubMed: 24565445]
48. Chandrasekaran S, Giang UB, King MR, DeLouise LA. Microenvironment induced spheroid to sheeting transition of immortalized human keratinocytes (HaCaT) cultured in microbubbles formed in polydimethylsiloxane. Biomaterials. 2011; 32:7159–7168. [PubMed: 21724250]

49. Agastin S, Giang UB, Geng Y, Delouise LA, King MR. Continuously perfused microbubble array for 3D tumor spheroid model. Biomicrofluidics. 2011; 5:24110. [PubMed: 21716809]
50. Chandrasekaran S, Geng Y, DeLouise LA, King MR. Effect of homotypic and heterotypic interaction in 3D on the E-selectin mediated adhesive properties of breast cancer cell lines. Biomaterials. 2012; 33:9037–9048. [PubMed: 22992472]
51. Shen K, Lee J, Yarmush ML, Parekkadan B. Microcavity substrates casted from self-assembled microsphere monolayers for spheroid cell culture. Biomed. Microdev. 2014; 16:609–615.
52. Desai SP, Freeman DM, Voldman J. Plastic masters-rigid templates for soft lithography. Lab Chip. 2009; 9:1631–1637. [PubMed: 19458873]
53. Choi SW, Cheong IW, Kim JH, Xia Y. Preparation of uniform microspheres using a simple fluidic device and their crystallization into close-packed lattices. Small. 2009; 5:454–459. [PubMed: 19189332]
54. Succi, S. The Lattice-Boltzmann Equation. Oxford University Press; 2001.
55. Chen S, Doolen GD. Lattice boltzmann method for fluid flows. Ann. Rev. Fluid Mech. 1998; 30:329–364.
56. Bhatnagar PL, Gross EP, Krook M. A model for collision processes in gases I Small amplitude processes in charged and neutral one-component systems. Phys. Rev. 1954; 94:511–525.
57. www.palabos.org
58. Zou Q, He X. On pressure and velocity boundary conditions for the lattice Boltzmann BGK model. Phys. Fluids. 1997; 9:1591–1598.
59. www.paraview.org
60. wci.llnl.gov/codes/visit/
61. Lee J, Wang JB, Bersani F, Parekkadan B. Capture and printing of fixed stromal cell membranes for bioactive display on PDMS surfaces. Langmuir. 2013; 29:10611–10616. [PubMed: 23927769]
62. Parekkadan B, Tilles AW, Yarmush ML. Bone marrow-derived mesenchymal stem cells ameliorate autoimmune enteropathy independently of regulatory T cells. Stem Cells. 2008; 26:1913–1919. [PubMed: 18420833]

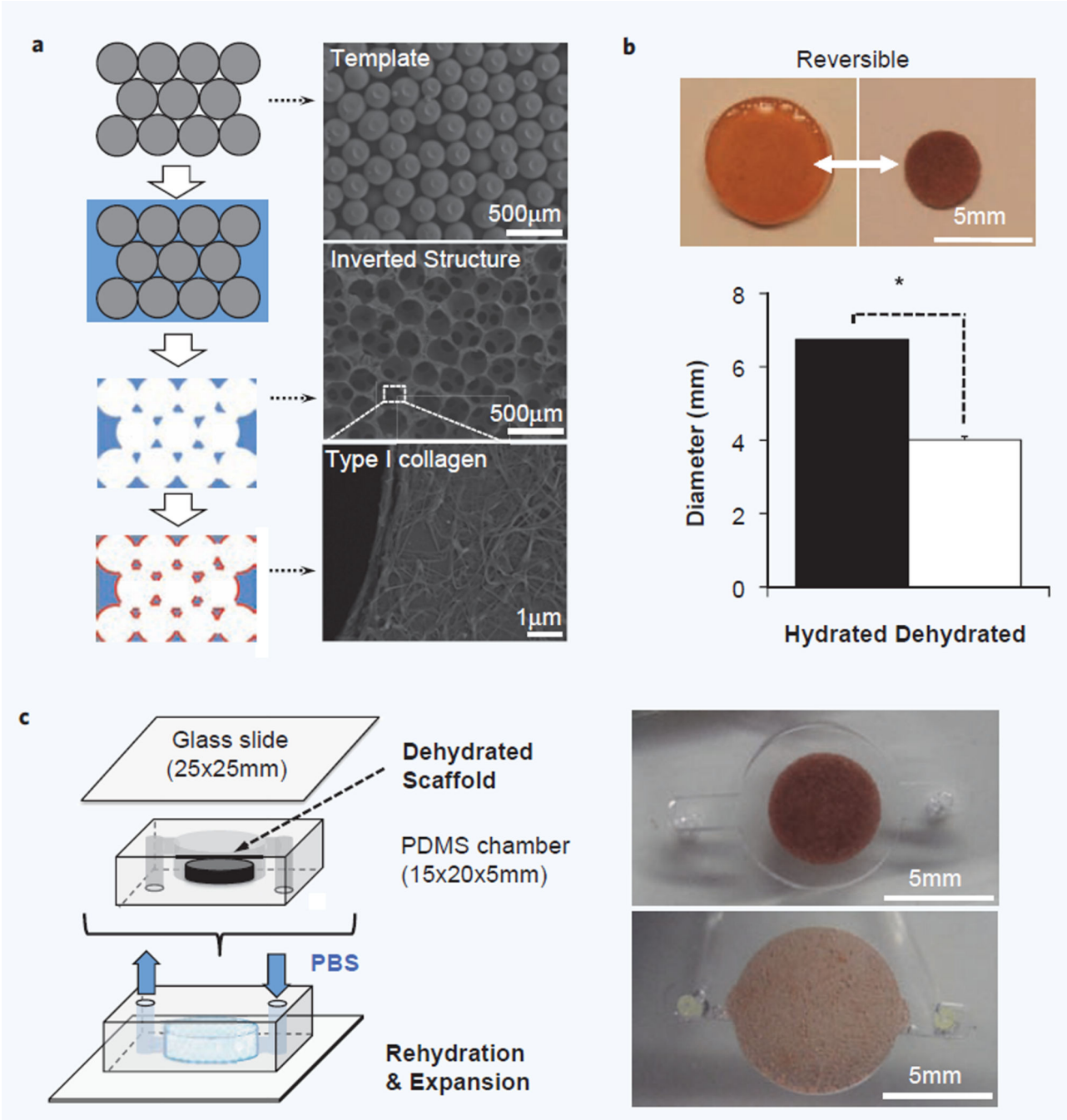

Figure 1.

Modular design of a microfluidic hydrogel scaffold. (**a**) Schematic of porous hydrogel scaffold fabrication procedure (*Left*) and corresponding SEM images in each stage (*Right*). Template structures were prepared with a narrow size distribution of microspheres and were infiltrated with hydrogel precursor solution prior to polymerization. Template beads were then selectively dissolved which left an inverted template structure to hydrogel matrix. Finally, the cavity surface was coated with Type I collagen to promote cell adhesion. (**b**) Hydrogel scaffolds undergo dramatic and fully reversible volume change between hydrated

and dehydrated states over 10 cycles. Dehydration of the hydrogel scaffold ($D = 4.01 \pm 0.09$ mm, $H \approx 0.6$ mm) shrank up to 78% of volume compared with its fully hydrated state ($D = 6.74 \pm 0.14$ mm, $H \approx 1.5$ mm), which is completely restored after rehydration ($n = 10$, $*p < 0.01$). (**c**) Schematic of microfluidic hydrogel scaffold preparation by integrating a hydrogel scaffold into a PDMS-based perfusion chamber. A dehydrated scaffold was placed in a PDMS chamber that has slightly smaller dimension to the fully hydrated scaffold and subsequently sealed with a glass slide. Micrographs below show the rehydrated scaffold in a chip completely fills the chamber space.

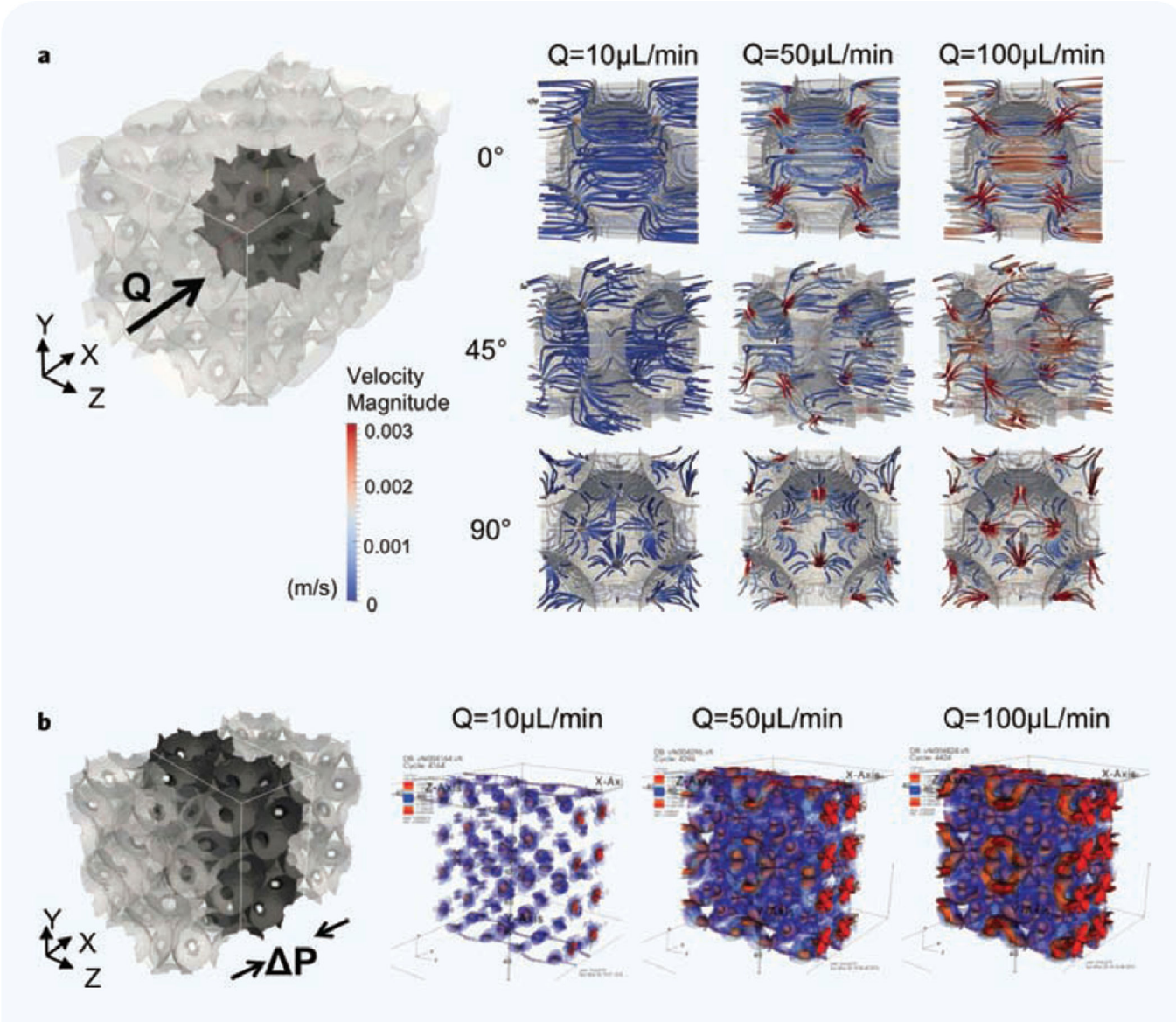

Figure 2.

Computational simulation of hydrodynamic and mechanical microenvironment in a microfluidic hydrogel scaffold. (**a**) Visualized 3D target volume and simulated fluidic perfusion in a single cavity at 10, 50 and 100 μL/min volumetric flow rate (*Q*) from three diffeent angles. The size of the computational box is 565.7 × 565.7 × 848.5 μm. Velocity magnatitue is meter per sec. (**b**) Visualized 3D target volume and the mechanical shear stress (Δ*P*) profile at the three flow rates in the central region of an integrated scaffold.

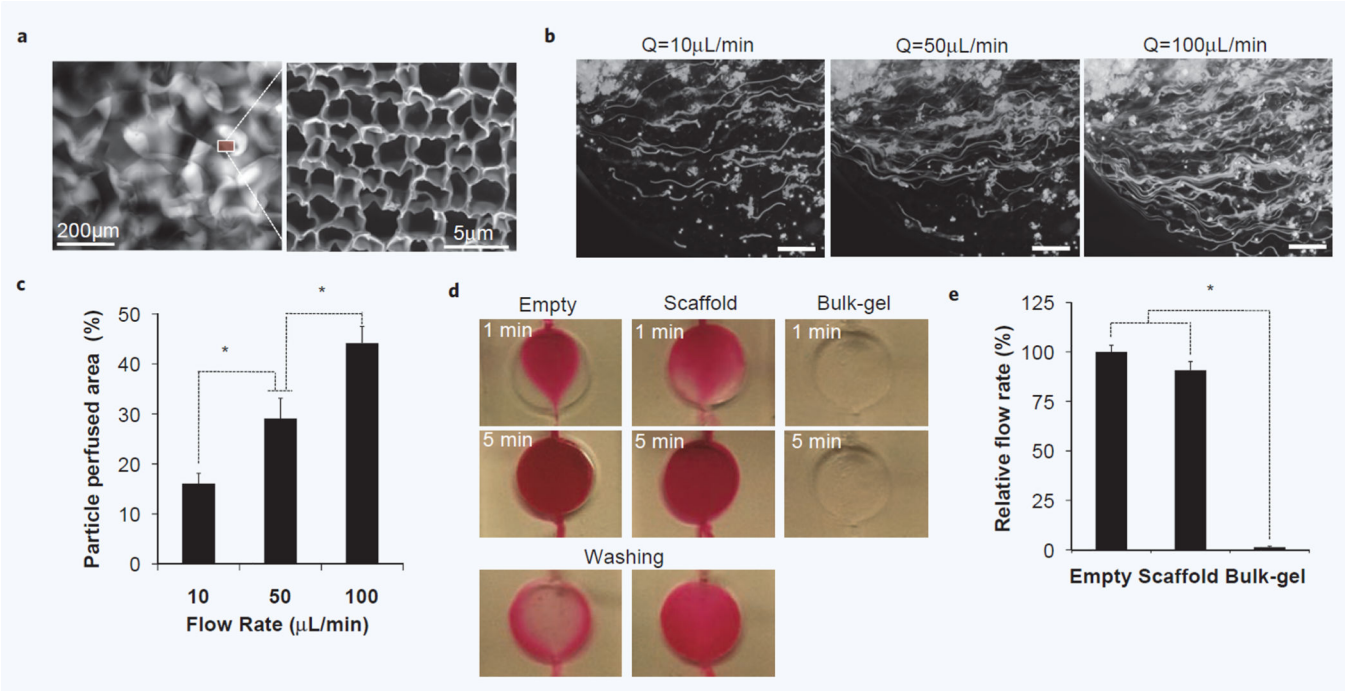

Figure 3.

Characterization of inter-scaffold hydrodynamic microenvironment. (**a**) Fluorescent image of micro-scale pores in a scaffold-chip visualized by injecting rhodamine solution (*Left*) and SEM image of subcellular scale pores in bulk hydrogel matrix (*Right*). (**b**) Perfusion profile of cellular size fluorescent microsparticles (D = 10∼15 μm) at three different flow rates. Streamline flows were captured by setting exposure time to 20 seconds. (Scale bar, 200 μm) (**c**) Quantitative comparision of perfused area at different flow rates. Increased flow rates perfuse not only more particles but also more area. (n = 5, *p < 0.05) (**d**) Perfusion profiles of rhodamine solution in an empty, scaffold and bulk-gel inserted chip under gravity-induced flow. No significant mass transport was detected in a bulk gel inserted chamber due to high fluidic resistance in the absence of macroscopic pores. Considerably longer retention of rhodamine molecule was observed in a scaffold-chip than an empty chamber. (**e**) Comparison of relative flow rates. Regularly arranged, hierarchical scale pores in hydrogel scaffold supports about 90% fluidic perfusion of an empty chamber (n = 5, *p < 0.1).

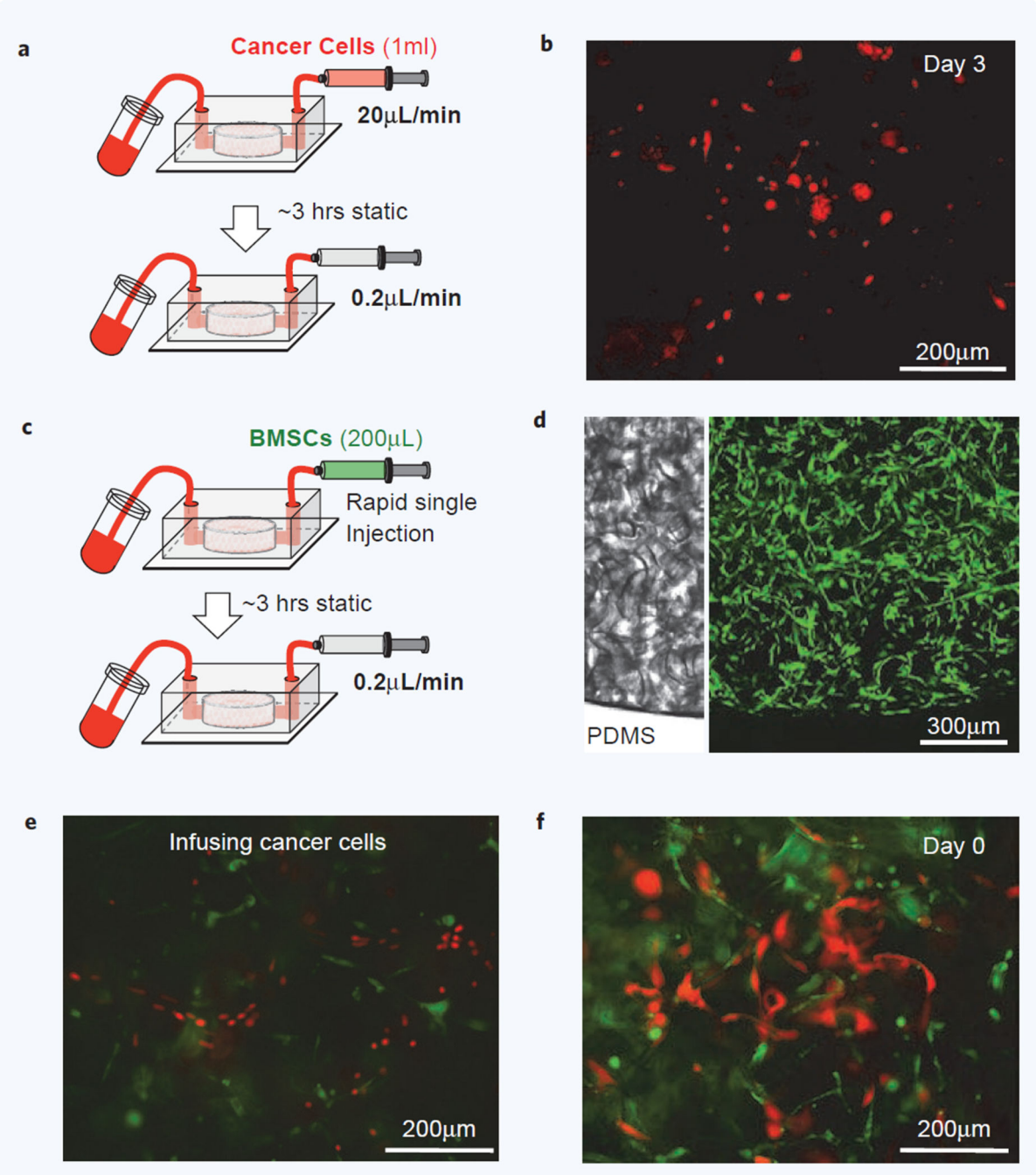

Figure 4.

Microfluidic 3D co-culture of human BMSCs and PC3 prostate cancer cells. (**a**) Schematic of PC3 human prostate cancer cell seeding into a scaffold-chip and subsequent perfusion culture. (**b**) Fluorescent image of Luc-GFP PC3 prostate cancer cells captured in a microfluidic scaffold after 3 days perfusion culture. PC3 cells are red colored to distinguish from human BMSCs. (**c**) Schematic of human BMSCs seeding into a scaffold-chip by single rapid injection and subsequent perfusion culture. (**d**) 3D confocal images of post 3 days perfusion culture show that BMSCs stably adhered on pore surface and well distributed both

axial and lateral directions of an integrated hydrogel scaffold. (**e,f**) Fluorescent images of co-culture microfluidic chip show engrafted human prostate tumor cells in 3D microenvironment.

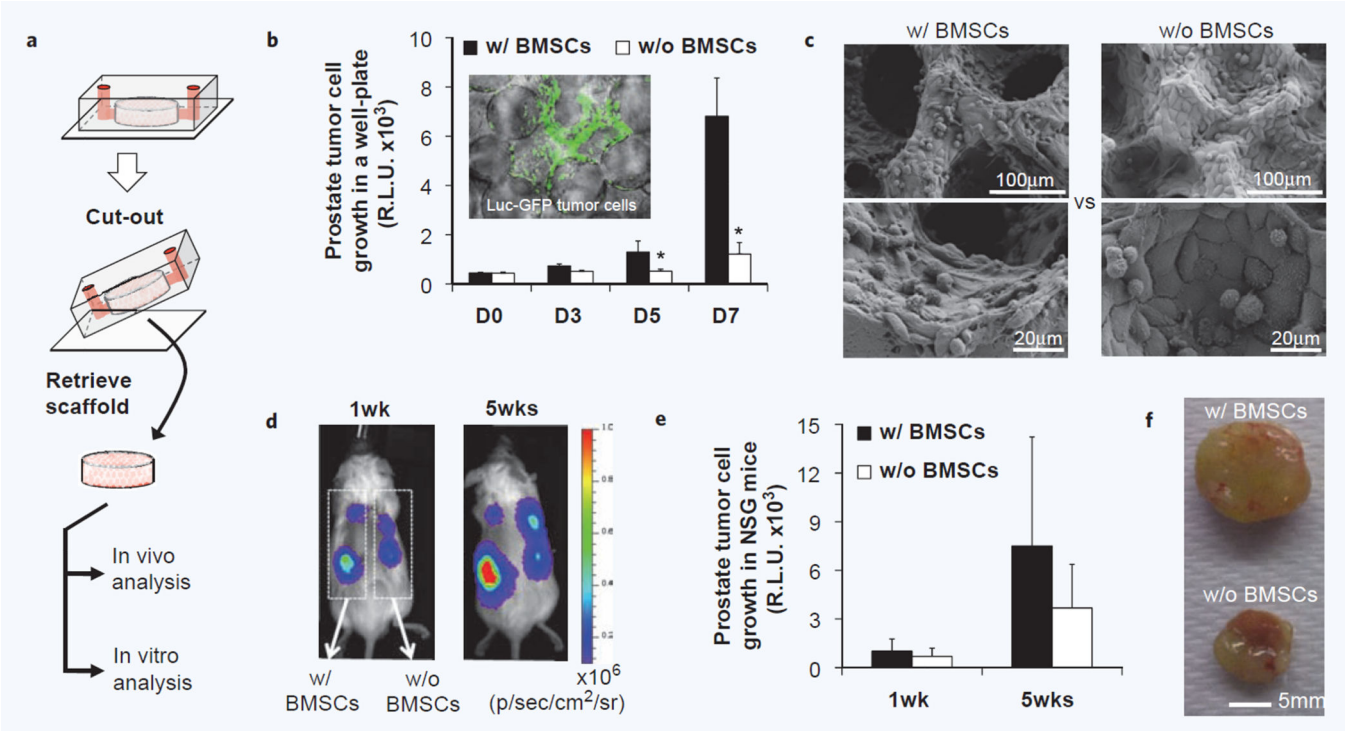

Figure 5.

Retrieval of hydrogel scaffold from microfluidic devices with retained xenograft capacity. (**a**) Schematic of retrieval of an integrated hydrogel scaffold from a microfluidic device for continues *in vitro* and *in vivo* analysis. (**b**) *In vitro* growth analysis of microfluidically captured Luc-GFP PC3 prostate tumor cells after transferring to a well plate using bioluminescent imaging ($n = 6$, $*p < 0.05$). Fluorescent image of tumor cells in a retrieved scaffold (*Inner panel*). (**c**) Morphological analysis of tumor cell growth with and without human BMSCs after 3 weeks *in vitro* culture. (**d**) *In vivo* growth analysis after subdermal implantation into immunodeficient mice using bioluminescent imaging. (**e**) Quantification of bioluminescent monitoring of tumor cell growth over 5 weeks *in vivo* ($n = 6$). (**f**) Gross image of explanted scaffolds 7 weeks after implantation.